Analytical and Numerical Solutions for Laminar Flow of the Non-Newtonian Ellis Fluid

SEIKICHI MATSUHISA and R. BYRON BIRD

University of Wisconsin, Madison, Wisconsin

Because of the apparent success in the use of the three-constant Ellis model to describe a wide variety of experimental data, a summary is given of analytical and numerical solutions for this model. The solutions include isothermal flow between flat plates, in tubes, in films, in annuli (axial, tangential, and radial) and nonisothermal flow in tubes with constant wall temperature and with constant heat flux at the tube wall.

Many polymers and polymer solutions exhibit the same type of variation of non-Newtonian viscosity with shear stress: In the limit of zero shear stress the non-Newtonian viscosity η approaches a constant value η_0. As the shear stress is increased, η decreases, and over a wide intermediate range of shear stress the logarithm of the non-Newtonian viscosity is linear in the logarithm of the shear stress (the so-called *power-law behavior*). Then at still higher shear stress there is some evidence that the non-Newtonian viscosity may approach a constant value η_∞.

Quite a few empirical expressions have been suggested to describe the non-Newtonian viscosity behavior (*8*). The simplest of these is the two-constant power-law model of Ostwald and de Waele, which can be used rather successfully for describing the wide intermediate range mentioned above. The model suffers from several major defects, however: one of the constants in the model has awkward dimensions, which in fact depend on the value of the other constant; the model gives $\eta_0 = \infty$; the model parameters cannot be used to construct a characteristic time for the fluid; and the constants determined from one flow system are different from those (for the same fluid) when determined in another flow system. Nonetheless the power-law description of non-Newtonian materials has proven useful (and will continue to be useful) in many problems.

The first three of the above objections (and to at least some extent the fourth) can be overcome simply by adding to the power law an extra term which describes the Newtonian behavior at low shear rates. This idea was apparently first suggested by Ellis (*22*). By an appropriate selection of the constants (*21*), one can write, for the simple case of shear flow with $v_x = v_x(y)$, $v_y = 0$, $v_z = 0$:

$$\tau_{yx} = -\eta \frac{dv_x}{dy} \tag{1}$$

$$\frac{1}{\eta} = \frac{1}{\eta_0}\left(1 + \left|\frac{\tau_{yx}}{\tau_{1/2}}\right|^{\alpha-1}\right) \tag{2}$$

The three constants appearing in the model are η_0, the value of the viscosity at zero shear; $\tau_{1/2}$, that value of the shear stress τ_{yx} for which $\eta = \eta_0/2$; and $\alpha - 1$ is the slope of the line obtained when $(\eta_0/\eta) - 1$ is plotted against $|\tau_{yx}/\tau_{1/2}|$ on log-log paper. For most polymers and polymer solutions α varies from 1 to 2. Extensive illustrations of the use of Equation (2) to describe non-Newtonian viscosity data have been given in the theses of Sadowski (*23*), Sutterby (*30*), and Turian (*31*). The model seems to be capable of reproducing the experimental data over about three decades of shear stress with an accuracy of the order of 5%.

Equations (1) and (2) can be generalized to more complicated flow patterns by the method suggested by Hohenemser and Prager (*14*)

$$\tau = -\eta\,(\nabla \mathbf{v} + (\nabla \mathbf{v})^\dagger) \tag{3}$$

$$\frac{1}{\eta} = \frac{1}{\eta_0}\left(1 + \left|\frac{\sqrt{\tfrac{1}{2}\,(\tau:\tau)}}{\tau_{1/2}}\right|^{\alpha-1}\right) \tag{4}$$

in which it is assumed that the fluid is incompressible. In the statement of the model in Equation (4), it has to be tacitly assumed that normal stresses are present only in those flow situations in which they would be present for a Newtonian fluid anyway. Thus for axial flow in a tube, one assumes that $\tau_{rr} = \tau_{\theta\theta} = \tau_{zz} = 0$, whereas for purely radial flow between coaxial cylinders $\tau_{rr} \neq 0$, $\tau_{\theta\theta} \neq 0$, $\tau_{zz} = 0$.

Several methods are available to determine the constants in the rheological model. Probably the simplest is to note that Equations (1) and (2) may be combined and put in dimensionless form as follows:

$$-\Gamma = T + T^a \qquad T > 0 \tag{5}$$

$$+\Gamma = (-T) + (-T)^a \qquad T < 0 \tag{6}$$

where $T = (\tau_{yx}/\tau_{1/2})$ and $\Gamma = (\eta_0/\tau_{1/2})\,(dv_x/dy)$. Consider now the case for $T > 0$. One then prepares a master plot of log T vs. log $(-\Gamma)$ for many values of α (see Figure 1). Then one plots the experimental data as log τ_{yx} vs. log $(-dv_x/dy)$ as obtained, say, from a cone-and-plate viscometer, with the same kind of logarithmic graph paper used. Now one slides the experimental data around on the master plot, keeping the coordinate axes of both graphs parallel, until the best fit is obtained. In this way one finds immediately a choice of α by noting which master curve fits the data the best. Furthermore, from the displacement of the axis of the experimental graph from the master plot, one can find $\tau_{1/2}$ (from the displacement in the τ_{yx} direction) and then η_0 (from the displacement in the $-dv_x/dy$ direction). This method, suggested by Professor W. E. Stewart of the University of Wisconsin, provides a convenient pictorial idea as to how well the model does indeed describe the experimental data.

The Ellis model was used by Gee and Lyon (*12*) in their study of molten polyethylene extrusion. In addition, the following work done in the Chemical Engineering Department at the University of Wisconsin has illustrated the usefulness of the model:

1. J. C. Slattery (*24, 25*) showed how Ellis model parameters could be used to correlate drag coefficients for flow around spheres.
2. D. M. Meter (*19, 20*) showed how turbulent tube flow data can be correlated with $\tau_{1/2}$.
3. A. G. Fredrickson (*9*) found that annular flow and tube flow could not both be described by the same set of power-law constants; Fredrickson (*10*) has suggested that the Ellis model would be more satisfactory, and subsequent work of McEachern (*17*) and Ashare and Bird (*1*) has seemed to indicate this.
4. R. M. Turian (*31*) has shown how the Ellis model may be used to describe the fall of spheres in tubes of different internal diameters, thereby systematizing the wall-correction formulas for the falling-ball viscometer. He has also obtained equations for the temperature dependence of the Ellis model parameters. Furthermore, he has obtained analytical solutions for the problem of viscous heating of an Ellis fluid in a cone-and-plate viscometer.
5. T. J. Sadowski (*23*) has shown that the flow of polymer solutions in porous media can be described with the Ellis model used for the fluid and the capillary model for the porous medium, that is, by using the method suggested on p. 206 of reference *8*. (The power-law model used there was, however, found to be unsatisfactory.) The resulting Ellis analogue of the Blake-Kozeny equation was found experimentally to be valid for slow flow, for which the characteristic time for the fluid ($\eta_0/\tau_{1/2}$) is small with respect to the characteristic time for the flow (D_p/v_0), where D_p is the particle diameter and v_0 is the superficial velocity. For more rapid flow, viscoelastic effects were noticeable, and these could be accounted for by introducing an additional dimensionless ratio $\eta_0 v_0/D_p\tau_{1/2}$ into the correlation. This provides an illustration of the use of the Ellis parameters to describe viscoelastic effects (*5*).
6. J. L. Sutterby (*30*) has shown that the explanation of the experimental data for converging sections is greatly facilitated by using a model which incorporates a zero-shear viscosity η_0 [although he used a function different from that in Equation (2)].
7. J. C. Biery (*3*) studied the non-Newtonian oscillating manometer; although he did not use the Ellis model in his analysis, his results seem to indicate that models of the type of Equation (2) can be used even for unsteady state systems as long as a characteristic time for the flow system (for example, the time for one manometer oscillation) is large compared with a characteristic time of the fluid (for example, $\eta_0/\tau_{1/2}$).

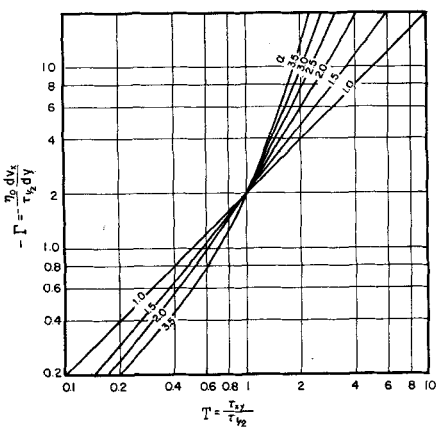

Fig. 1. Master plot of Ellis model from Equation (5).

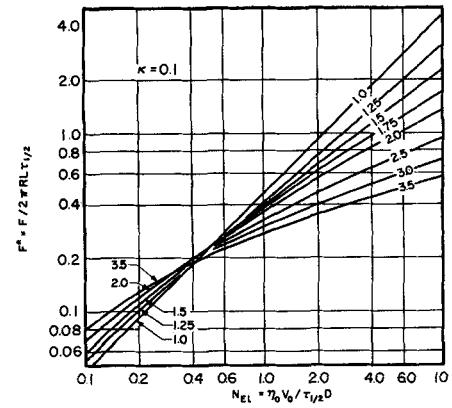

Fig. 2. Force-velocity relation for axial flow in annulus with inner tube moving axially.

This series of experimental studies seems to indicate that the Ellis model is a very useful empirical relation for engineering applications, either for analytical and numerical solutions, or for dimensional analysis purposes.

The Ellis model belongs to the class of models known as generalized Newtonian fluids. Such fluids cannot be used to describe analytically normal stress phenomena such as Weissenberg effects, nor can they describe high frequency oscillatory phenomena. Nonetheless the Ellis parameters may be useful in empirical characterization of such viscoelastic phenomena (as in the Sadowski packed-bed experiment described above). That this should be true may be seen as follows. Viscoelastic models, capable of describing the whole spectrum of rheological behavior, often simplify for viscometric flows, giving non-Newtonian viscosities which contain a zero-shear viscosity η_0, a characteristic time, and perhaps one or more dimensionless constants [this is true, for example, of the three-constant Oldroyd model (*33, 34*), the two-constant Spriggs-Bird model (*29*), the four-constant nonlinear generalized Maxwell model of Spriggs (*27, 28*), etc.]. In fact the last named model yields a non-Newtonian viscosity function which has a shape very similar to that of the Ellis model. This suggests, then, that the Ellis model parameters do contain hidden information about the viscoelastic behavior of the fluid and that it should be possible to obtain some experimental correlations of normal stress phenomena and oscillatory motion in terms of such parameters (*4, 5*).

The purpose of this article is to present a number of new solutions to flow problems with the Ellis model, some analytical, some numerical, and some approximate. To these are added, for convenience, several analytical solutions for simple systems just to make the summary as complete as possible. It is hoped that this summary will enable greater use to be made of this model, both in research and design. Perhaps it will also serve to catalyze others to present their data in terms of the model constants suggested here and to subject the model to further experimental test.

The solutions are divided into two major groups: isothermal flow and nonisothermal flow. The solutions in the latter category assume that the model parameters are temperature independent; hence, they can be regarded only as limiting solutions. In the near future work will be available on the temperature dependence of the Ellis model parameters (*31*), and then these nonisothermal problems can be greatly extended.

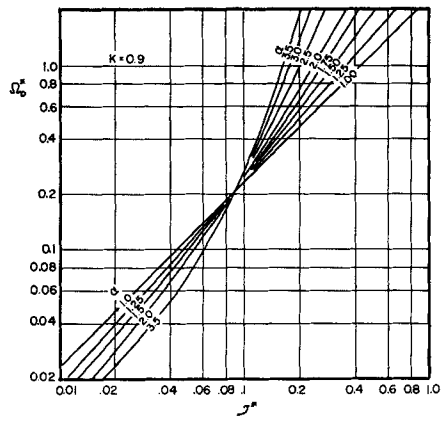

Fig. 3. Relation between torque and angular velocity in tangential flow in an annulus with $\kappa = 0.9$

ISOTHERMAL FLOW

Flow between Flat Plates:
$[v_x = v_x(x),\ v_y = 0,\ v_z = 0;\ p = p(z)]$

The fluid flows in the z direction, as a result of a pressure gradient, in a horizontal slot bounded by the planes $x = \pm B$ and $y = 0, W$. The slot has a length L. It is assumed that $W >> B$, so that v_z does not vary appreciably with y. The velocity distribution and volume rate of flow are given by

$$v_z = \frac{B\tau_B}{2\eta_0}\left\{\left[1-\left(\frac{x}{B}\right)^2\right] + \frac{2}{\alpha+1}\left(\frac{\tau_B}{\tau_{1/2}}\right)^{\alpha-1}\left[1-\left(\frac{x}{B}\right)^{\alpha+1}\right]\right\} \quad (7)$$

$$Q = \frac{2B^2W\tau_B}{3\eta_0}\left[1+\frac{3}{\alpha+2}\left(\frac{\tau_B}{\tau_{1/2}}\right)^{\alpha-1}\right] \quad (8)$$

in which $\tau_B = [p(0) - p(L)]B/L$ is the shear stress at the wall.

Flow in Circular Tubes:
$[v_z = v_z(r),\ v_\theta = 0,\ v_r = 0;\ p = p(z)]$

The fluid flows in the z direction, as a result of a pressure gradient, in a circular tube of radius R and length L. The velocity distribution and volume flow rate are

$$v_z = \frac{R\tau_R}{2\eta_0}\left\{\left[1-\left(\frac{r}{R}\right)^2\right] + \frac{2}{\alpha+1}\left(\frac{\tau_R}{\tau_{1/2}}\right)^{\alpha-1}\left[1-\left(\frac{r}{R}\right)^{\alpha+1}\right]\right\} \quad (9)$$

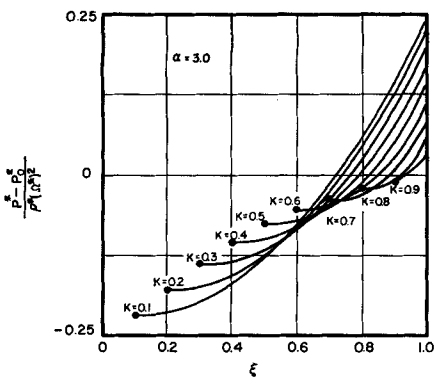

Fig. 4. Pressure distribution in tangential flow in annuli ($\alpha = 3.0$) when the inner cylinder is stationary.

$$Q = \frac{\pi R^3\tau_R}{4\eta_0}\left[1+\frac{4}{\alpha+3}\left(\frac{\tau_R}{\tau_{1/2}}\right)^{\alpha-1}\right] \quad (10)$$

in which $\tau_R = [p(0) - p(L)]R/2L$ is the shear stress at the wall.

Flow in a Film Flowing along an Inclined Plate:
$[v_z = v_z(x)]$

The fluid flows down an inclined surface which makes an angle β with the vertical (that is, $\beta = 0$ corresponds to a vertical surface). The z direction is in the direction of flow along the inclined plane, and x is perpendicular to the plane, with $x = 0$ at the surface of the liquid and $x = B$ the wetted surface of the plate. The width of the plate is W. The velocity distribution is given by Equation (7) with τ_B replaced by $\rho gB\cos\beta$. The volume rate of flow is given by Equation (8) with τ_B replaced by $\rho gB\cos\beta$ and the right-hand side multiplied by ½ to account for the fact that the film thickness is B whereas the slot thickness was $2B$.

Axial Flow in Fixed Annuli: $[v_z = v_z(r),\ v_\theta = 0,\ v_r = 0;\ p = p(z)]$

A fluid is flowing axially in the region between two coaxial cylinders of radii κR and R (where $\kappa < 1$). If κ is only slightly less than unity, the results for flow between flat plates can be used, with appropriate modification: replace x by $r - (\frac{1}{2})(1+\kappa)R$, B by $(\frac{1}{2})(1-\kappa)R$, and W by $2\pi R$. The resulting formula for Q will, of course, be somewhat inaccurate because curvature effects have been neglected. It has been shown (*1*) that for power-law fluids, the analytical results of Fredrickson and Bird (*11*) may be very closely approximated by multiplying the power-law plane slot formula by a Newtonian curvature correction factor (*8*). Hence, the authors recommend that for annuli with κ greater than about 0.6

$$Q = \frac{\pi R^4\Delta p\epsilon^8}{6\eta_0 L}\left[1+\frac{3}{\alpha+2}\left(\frac{\Delta p\epsilon R}{2\tau_{1/2}L}\right)^{\alpha-1}\right]\cdot \left(1-\frac{1}{2}\epsilon+\frac{1}{60}\epsilon^2+\ldots\right) \quad (11)$$

may be a useful empiricism; here $\epsilon = 1 - \kappa$. A complete numerical solution of axial flow in an annulus has been made by D. W. McEachern and will be published elsewhere with a comparison of experimental data (*18*).

Axial Flow in Annuli with Inner Tube Moving Axially:
$[v_z = v_z(r),\ v_\theta = 0,\ v_r = 0,\ p = \text{constant}]$

A fluid is flowing tangentially in the region between two coaxial cylinders of radii κR and R (where $\kappa < 1$). The cylinder at $r = R$ is fixed and that at $r = \kappa R$ moves axially with a velocity v_0. The velocity distribution is

$$v_z = \frac{\tau_{1/2}R}{\eta_0}\left[C\ln\frac{1}{\xi}+\frac{C^\alpha}{\alpha-1}\left(\frac{1}{\xi^{\alpha-1}}-1\right)\right] \quad (12)$$

where $\xi = r/R$, and the dimensionless constant C is obtained from the requirement that $v_z = v_0$ at $\xi = \kappa$. The force F on the inner tube to maintain the axial motion through an outer tube of length L is given implicitly by

$$v_0 = \frac{\tau_{1/2}R}{\eta_0}\left[\left(\frac{F}{2\pi RL\tau_{1/2}}\right)\ln\frac{1}{\kappa} + \frac{1}{\alpha-1}\left(\frac{F}{2\pi RL\tau_{1/2}}\right)^\alpha\left(\frac{1}{\kappa^{\alpha-1}}-1\right)\right] \quad (13)$$

This result is shown in Figure 2 for $\kappa = 0.1$, where $F^* = F/2\pi RL\tau_{1/2}$ is plotted against $N_{Re} = \eta_0 v_0/2\tau_{1/2}R$.

Tangential Flow in Annuli: $[v_\theta = v_\theta(r),\ v_r = v_z = 0;\ p = p(r)]$

A fluid is flowing tangentially in the region between two coaxial cylinders of radii κR and R and of length L ($\kappa < 1$); the inner cylinder at $r = \kappa R$ rotates with an angular velocity Ω_i, whereas the outer one rotates with an angular velocity Ω_o. The angular velocities Ω_i and Ω_o are considered to be positive when they are counterclockwise (positive θ direction) and negative when they are clockwise (negative θ direction).

Velocity Distribution. The angular velocity $\Omega = v_\theta/r$ at any position r is expressed as

$$\pm (\Omega - \Omega_i)(\eta_0/\tau_{1/2}) = \frac{1}{2}\left(\frac{\pm T}{2\pi L \tau_{1/2} R^2}\right)\left(\frac{1}{\kappa^2} - \frac{1}{\xi^2}\right) + \frac{1}{2\alpha}\left(\frac{\pm T}{2\pi L \tau_{1/2} R^2}\right)^a \left(\frac{1}{\kappa^{2a}} - \frac{1}{\xi^{2a}}\right) \quad (14)$$

in which $\xi = r/R$, and T is the torque which has to be applied to the outer cylinder to maintain the motion; the torque is regarded as positive if it is applied in the positive θ direction. The upper signs apply when $\Omega_o \geqq \Omega_i$ and $T > 0$, whereas the lower signs apply when $\Omega_o \leqq \Omega_i$ and $T < 0$.

The relation between the torque T and the angular velocity of the outer cylinder Ω_o is given by

$$\Omega_o{}^* = \frac{T^*}{2}\left(\frac{1}{\kappa^2} - 1\right) + \frac{(T^*)^a}{2\alpha}\left(\frac{1}{\kappa^{2a}} - 1\right) \quad (15)$$

in which $\Omega_o{}^* = \pm (\Omega_o - \Omega_i)(\eta_0/\tau_{1/2})$ and $T^* = (\pm T/2\pi L \tau_{1/2} R^2)$. A sample set of curves of $\Omega_o{}^*$ vs. T^* is shown in Figure 3 for $\kappa = 0.9$. Curves of this type can be used for determining the constants in the Ellis model from measurements of torque and angular velocity in a coaxial annular viscometer.

Pressure Distribution. The method of Bird, Curtiss, and Stewart (7) for the Newtonian fluid can be extended to the Ellis fluid. The pressure distribution is expressed as

$$\frac{p^* - p_o{}^*}{\rho^*} = \frac{E^2}{2}\xi^2 - \frac{F^2}{2}\xi^{-2} + \frac{EG}{\alpha - 1}\xi^{-(2\alpha-2)} - \frac{FG}{\alpha}\xi^{-2\alpha} - \frac{G^2}{2(2\alpha-1)}\xi^{-(4\alpha-2)} - 2EF\ln\xi - \frac{1}{1-\kappa^2}\left\{\frac{E^2}{4}(1-\kappa^4) + F^2\ln\kappa + \frac{G^2}{4(2\alpha-1)(\alpha-1)}(1-\kappa^{-(4\alpha-4)}) + 2EF\kappa^2\ln\kappa + EF(1-\kappa^2) + \frac{FG}{\alpha(\alpha-1)}(1-\kappa^{-(2\alpha-2)}) - \frac{EG}{(\alpha-1)(\alpha-2)}(1-\kappa^{-(2\alpha-4)})\right\} \quad (16)$$

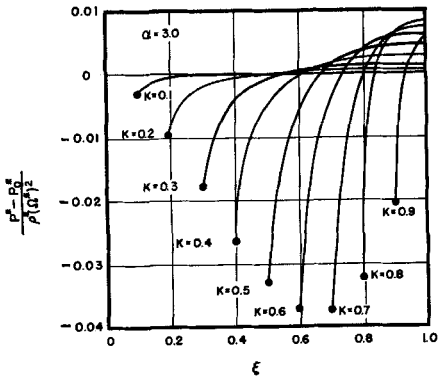

Fig. 5. Pressure distribution in tangential flow in annuli ($\alpha = 3.0$) when the outer cylinder is stationary.

in which p^*, ρ^*, E, F, and G are dimensionless quantities: $p^* = p/\tau_{1/2}$, $\rho^* = \rho\eta_0{}^2/R^2\tau_{1/2}$, $E = \eta_0\Omega_i/\tau_{1/2} \pm T^*/2\kappa^2 \pm (T^*)^a/2\alpha\kappa^{2a}$, $F = \pm T^*/2$, and $G = \pm (T^*)^a/2\alpha$, in which positive and negative signs correspond to $\Omega_o \geqq \Omega_i$ and $\Omega_o < \Omega_i$, respectively. Three important limiting cases for the pressure distribution are

1. $\Omega_i = \Omega_o = \Omega$

$$\frac{p^* - p_o{}^*}{\rho^* E^2} = \frac{\xi^2}{2} - \frac{1}{4}(1 + \kappa^2) \quad (17)$$

The result is exactly the same as that for the Newtonian case if one plots $(p^* - p_o{}^*)/\rho^* E^2$ vs. ξ instead of $(p - p_0)/\rho_0 R\Omega^2$ vs. ξ.

2. $\Omega_i = 0, \Omega_o \neq 0$

In Equation (16), the coefficient E becomes $T^*/2\kappa^2 + (T^*)^a/2\alpha\kappa^{2a}$. The result of numerical calculations is plotted in Figure 4 for $\alpha = 3.0$. The resulting plot is very nearly the same as the plot of $(p - p_0)/\rho_0\Omega_o{}^2R^2$ vs. ξ for the Newtonian case.

3. $\Omega_i \neq 0, \Omega_o = 0$

The result of numerical calculations is plotted in Figure 5 for $\alpha = 3.0$. The resulting plot is also nearly the same as the plot of $(p - p_0)/\rho_0\Omega_i{}^2R^2$ vs. ξ for the Newtonian case.

Radial Flow in Annuli: $[v_r = v_r(r),\ v_\theta = v_z = 0;\ p = p(r)]$

A fluid is flowing radially in the region between two porous coaxial cylinders of radii R and aR, both of which are stationary ($a > 1$).

From the equation of continuity, it is found that $v_r = \pm Q/2\pi rL$ where the upper sign corresponds to outward flow and the lower sign to inward flow.

Shear Stress Distribution. For the above velocity distribution $\tau_{rr} = -\tau_{\theta\theta} = \pm \dfrac{\eta Q}{\pi r^2 L}$, and all other components of the stress tensor are zero. The stress distribution is then

$$\left(\frac{Q}{2\pi L r^2}\right)\left(\frac{\eta_0}{\tau_{1/2}}\right) = \left(\pm\frac{\tau_{rr}}{\tau_{1/2}}\right) + \left(\pm\frac{\tau_{rr}}{\tau_{1/2}}\right)^a \quad (18)$$

The stresses as functions of the flow rates can be obtained for various values of α by using Figure 1 with appropriate changes in the labelling of the axes.

Pressure Distribution. When use is made of the fact that $\tau_{\theta\theta} = -\tau_{rr}$, the r component of the equation of motion becomes

$$\frac{1}{2}\rho\frac{d}{dr}(v_r{}^2) = -\frac{dp}{dr} - \frac{1}{r^2}\frac{d}{dr}(r^2\tau_{rr}) \quad (19)$$

This equation may be integrated to give, in dimensionless form

$$p^*|_\xi - p^*|_1 = \frac{N_{Re_{1/2}}}{2}\left(1 - \frac{1}{\xi^2}\right) + (T|_1 - T|_\xi) - 2\int_1^\xi \frac{T}{\xi}d\xi \quad (20)$$

in which $p^* = p/\tau_{1/2}$, $T^* = \tau_{rr}/\tau_{1/2}$, and $N_{Re_{1/2}} = \rho(v_r|_R)^2/\tau_{1/2}$. For $\alpha = 2$, an analytical expression can be obtained:

$$p^*|_\xi - p^*|_1 = \frac{N_{Re_{1/2}}}{2}\left(1 - \frac{1}{\xi^2}\right)$$

$$+\frac{1}{2}\left(\frac{\sqrt{\xi^2+16N_{El}}}{\xi}-\sqrt{1+16N_{El}}\right)$$

$$+\ln\frac{\xi(1+\sqrt{1+16N_{El}})}{\xi+\sqrt{\xi^2+16N_{El}}} \quad (21)$$

in which N_{El}, the Ellis number, is defined as $N_{El} = \eta_0 v_r|_R/\tau_{1/2}D$, where $D = 2R$. The pressure distribution is shown in Figures 6 and 7; notice that the pressure difference can be either positive or negative depending on the values of the two dimensionless groups N_{El} and $N_{Re_{1/2}}$.

Flow in a Film on a Moving Wall

A solid wall immersed in an Ellis fluid moves upward with constant velocity v_0, and the fluid also moves upward clinging to the wall as shown in Figure 8. The thickness of the film δ is a function both of the distance z above the fluid level and of the time t.

From an unsteady state mass balance

$$\frac{\partial}{\partial z}(<v_z>\delta)+\frac{\partial\delta}{\partial t}=0 \quad (22)$$

or in dimensionless form

$$\frac{\partial\delta^*}{\partial t^*}+\frac{\partial<v_z^*>\delta^*}{\partial\zeta}=0 \quad (23)$$

in which dimensionless quantities are $v_z^* = v_z/v_0$, $\delta^* = \rho g\delta/\tau_{1/2}$, $t^* = \tau_{1/2}t/\eta_0$, and $\zeta = z\tau_{1/2}/v_0\eta_0$. The film thickness δ can be obtained by solving Equation (22), or (23), with the boundary condition that $\delta = 0$ at $z = v_0t$ (or $\delta^* = 0$ at $\zeta = t^*$).

The approximate value of the average velocity $<v_z^*>$ can be obtained from the momentum flux distribution and Equations (1) and (2) with the assumption that $v_x = 0$. The momentum flux distribution is

$$\tau_{xz} = \rho g(\delta - x) \quad \text{or} \quad T = \delta^*(1-\xi) \quad (24)$$

in which $T = \tau_{xz}/\tau_{1/2}$ and $\xi = x/\delta$. Equations (1) and (2) in dimensionless form are

$$\frac{dv_z^*}{d\xi} = -\delta^* K[T + T^a] \quad (25)$$

in which $K = \dfrac{(\tau_{1/2})^2}{\eta_0 v_0 \rho g}$. From Equations (24) and (25) and the boundary condition, at $\xi = 0$, $v_z^* = 1$

$$v_z^* = 1 - K\left[\frac{(\delta^*)^2}{2}\{1-(1-\xi)^2\}+\frac{(\delta^*)^{(a+1)}}{a+1}\{1-(1-\xi)^{a+1}\}\right] \quad (26)$$

and

$$<v_z^*> = \int_0^1 v_z^* d\xi = 1 - K\left(\frac{(\delta^*)^2}{3}+\frac{(\delta^*)^{(a+1)}}{a+2}\right) \quad (27)$$

Substitution of this expression for $<v_z^*>$ into Equation (23) gives the following differential equation for the film thickness:

$$\frac{\partial\delta^*}{\partial t^*}+\{1-K((\delta^*)^2+(\delta^*)^{(a+1)})\}\frac{\partial\delta^*}{\partial\zeta}=0 \quad (28)$$

This equation is solved (26) for the above-mentioned boundary condition to give

$$\zeta = [1-K(\delta^*)^2+(\delta^*)^{(a+1)})]t^* \quad (29)$$

From Equation (29), the film thickness at steady state is constant for all ζ and given by the root of the following equation:

$$(\delta^*)^{(a+1)}+(\delta^*)^2 = 1/K \quad (30)$$

In the limit as a approaches 1, the result for a Newtonian fluid of viscosity $\eta_0/2$ is obtained, namely $\delta = \sqrt{v_0\eta_0/2\rho g}$.

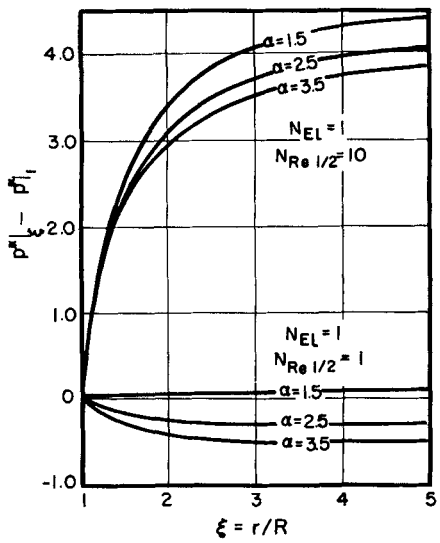

Fig. 6. Pressure distribution in outward radial flow in annuli with $N_{El} = 1.0$.

NONISOTHERMAL FLOW

In all of the cases discussed here the authors consider steady state flow in a tube of circular cross section (with z and r as the axial and radial coordinates, respectively). In the region $z < 0$, the velocity distribution is considered to be already fully developed. The temperature of the fluid at $z = 0$ is $\theta = 0$, whereas the tube wall for $z > 0$ is either held at the constant temperature $\theta = \theta_0$ or else there is a constant heat flux $q_0 = -k(\partial\theta/\partial r)|_{r=R}$. The temperature at any position can be calculated from the equation of energy (with the appropriate boundary conditions):

$$\rho\hat{C}_p v_z\frac{\partial\theta}{\partial z} = k\frac{1}{r}\frac{\partial}{\partial r}\left(r\frac{\partial\theta}{\partial r}\right) \quad (31)$$

The local heat transfer coefficient h is defined by

$$h(z) = \frac{-k\left.\dfrac{\partial\theta}{\partial r}\right|_{r=R}}{\theta(z,R)-<\theta>} \quad (32)$$

or in dimensionless form

$$N_{Nu} = \frac{hD}{k} = \frac{-2\left.\dfrac{\partial\theta}{\partial\xi}\right|_{\xi=1}}{\theta|_{\xi=1}-<\theta>} \quad (33)$$

In these expressions the average temperature over the cross section is defined as follows:

$$<\theta> = \frac{\int_0^R r\,v_z\,\theta\,dr}{\int_0^R r\,v_z\,dr} \quad (34)$$

Circular Tubes with Constant Wall Heat Flux

Thermal Entrance Region. The Nusselt number is expressed as (6)

$$N_{Nu} = \frac{\Gamma\left(\frac{2}{3}\right)}{9^{1/3}}\left(\frac{\gamma_R D^3}{z\chi}\right)^{1/3} \quad (35)$$

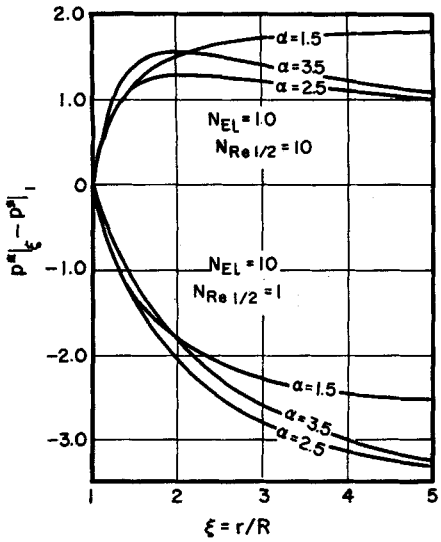

Fig. 7. Pressure distribution in outward radial flow in annuli with $N_{El} = 10$.

where χ is the thermal diffusivity of the fluid, Γ is the Gamma function, and $\gamma_R = -(dv_z/dr)|_{r=R}$.
For an Ellis fluid

$$\gamma_R = \frac{\tau_R}{\eta_0}(1 + T_R^{\alpha-1}) \tag{36}$$

in which T_R is the dimensionless shear stress at the wall $T_R = \tau_R/\tau_{1/2}$.

Substitution of Equation (36) into Equation (35) gives

$$N_{Nu} = \frac{\Gamma\left(\frac{2}{3}\right)}{9^{1/3}}\left(\frac{\tau_R(1 + T_R^{\alpha-1})D^3}{\chi\eta_0 z}\right)^{1/3} \tag{37}$$

for the Nusselt number.

Thermally Fully Developed Region. The asymptotic Nusselt number is dependent only on the velocity profile and can be expressed as (*16*)

$$(N_{Nu})^{-1} = 2\int_0^1 \frac{1}{\xi}\left[\int_0^\xi \xi' v_z^*(\xi')\,d\xi'\right]^2 d\xi \tag{38}$$

For an Ellis fluid $v_z^* = v_z/\langle v_z\rangle = \pi R^2 v_z/Q$ is given by Equations (9) and (10); substitution into Equation (38) then gives

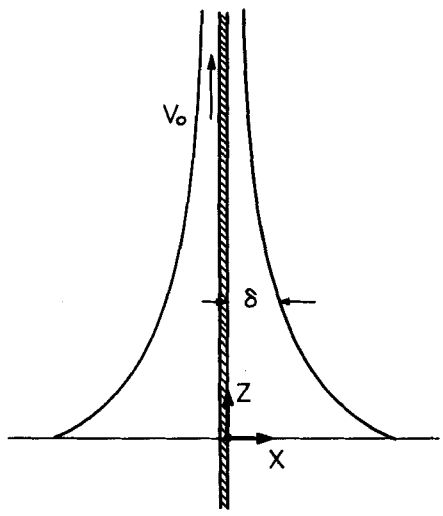

Fig. 8. Flow in a film on a moving wall.

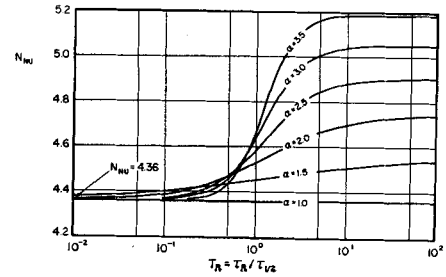

Fig. 9. Nusselt numbers for heat transfer in tube flow of an Ellis fluid (constant wall heat flux; thermally fully developed region).

$$(N_{Nu})^{-1} = \frac{\frac{11}{48} + \left(\frac{2T_R^{\alpha-1}}{\alpha+1}\right)f_1 + \left(\frac{2T_R^{\alpha-1}}{\alpha+1}\right)^3 f_2}{\left(1 + \frac{4T_R^{\alpha-1}}{\alpha+3}\right)^2}$$

with

$$f_1 = \frac{2}{3} - \frac{8}{(\alpha+3)(\alpha+5)} + \frac{4}{(\alpha+3)(\alpha+7)}$$

$$f_2 = \frac{1}{2} - \frac{8}{(\alpha+3)(\alpha+5)} + \frac{4}{(\alpha+3)^3} \tag{39}$$

The Nusselt numbers for various α's and T_R's computed in accordance with Equation (39) are shown in Figure 9.

Circular Tubes with Constant Wall Temperature

Thermal Entrance Region. The Nusselt number is expressed as (*6*)

$$N_{Nu} = \frac{1}{\Gamma\left(\frac{4}{3}\right)9^{1/3}}\left(\frac{\gamma_R D^3}{z\chi}\right)^{1/3} \tag{40}$$

For an Ellis fluid, once again Equation (36) is used to obtain

$$N_{Nu} = \frac{1}{\Gamma\left(\frac{4}{3}\right)9^{1/3}}\left(\frac{\tau_R(1 + T_R^{\alpha-1})D^3}{\chi\eta_0 z}\right)^{1/3} \tag{41}$$

Thermally Fully Developed Region. General solutions for Equation (31) may be obtained by the method of separation of variables:

$$\theta(\xi,\zeta) - \theta_0 = X(\xi)\,Z(\zeta) \tag{42}$$

Substitution of Equation (42) into Equation (31) gives equations for $X(\xi)$ and $Z(\zeta)$:

$$\frac{dZ}{d\zeta} = -\lambda^2 Z$$

$$\frac{1}{\xi}\frac{d}{d\xi}\left(\xi\frac{dX}{d\xi}\right) + \lambda^2 v_z^* X = 0 \tag{43}$$

The X equation is to be solved with the conditions that at $\xi = 0$, X is finite, and at $\xi = 1$, X is zero. In the thermally fully developed region, the Nusselt number is just equal to the first eigenvalue obtained from the X equation (*2*); that is

$$\lim_{\zeta\to\infty} Nu = \lambda_1^2 \tag{44}$$

For an Ellis fluid, $v_z^* = v_z/\langle v_z\rangle = \pi R^2 v_z/Q$ is expressed by Equations (9) and (10). The Nusselt numbers are calculated by Stodola and Vianello's method (*13*).

In Stodola and Vianello's method, a tentative temperature distribution, such as

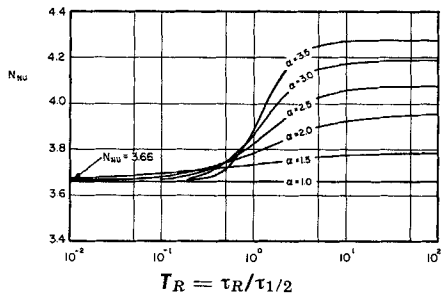

Fig. 10. Nusselt numbers for heat transfer in tube flow of an Ellis fluid (constant wall temperature; thermally fully developed region).

$$X_0 = \theta_0(1 - \xi^2) \tag{45}$$

is assumed. The first approximation for λ_1^2 is given by

$$\lambda_1^2 = \frac{\int_0^1 \xi v_z^* X_1(\xi) X_0(\xi)\, d\xi}{\int_0^1 \xi v_z^* [X_1(\xi)]^2\, d\xi} \tag{46}$$

in which $X_1(\xi)$ is the second approximation for the temperature distribution obtained by insertion of Equation (45) into Equation (43). The Nusselt numbers for various α's and T_R's are shown in Figure 10. The Nusselt numbers for the Ellis fluid at high shear rates indicate good agreement with the values for the power-law fluid given by Lyche and Bird (*15*) and Beek and Eggink (2).

ACKNOWLEDGMENT

Seikichi Matsuhisa is indebted to the Toyo Rayon Company of Japan for financial support during this work. R. Byron Bird wishes to acknowledge assistance provided by National Science Foundation grants G-11996 and GP 1875, and the A. C. S. Petroleum Research Fund Grant 1758-C.

NOTATION

a = ratio of radius of outer cylinder to that of inner cylinder
B = clearance of slot
$\hat{C}_p$ = heat capacity at constant pressure (per unit mass)
D = tube diameter
E = dimensionless parameter in Equation (16)
F = dimensionless parameter in Equation (16)
F = force
F^* = dimensionless force
G = dimensionless parameter in Equation (16)
g = gravitational acceleration
h = heat transfer coefficient
K = dimensionless parameter in Equation (25)
k = thermal conductivity
L = lengths of slot, tube, and annuli
N_{El} = Ellis number
N_{Nu} = Nusselt number
$N_{Re_{1/2}}$ = modified Reynolds number
p = pressure
p^* = dimensionless pressure
Q = volume flow rate
q_o = heat flux at tube wall
R = radius of tube
r = radial coordinate
T = dimensionless stress tensor
t = time
t^* = dimensionless time
$\mathcal{T}$ = torque
$\mathcal{T}^*$ = dimensionless torque
v = velocity
v^* = dimensionless velocity
$\langle v \rangle$ = average velocity
v_o = characteristic velocity
W = width of slot
x, y, z = rectangular coordinates
z = axial coordinate

Greek Letters

α = parameter in Ellis model
β = angle
γ_R = velocity gradient at tube wall
Γ = dimensionless velocity gradient
δ = film thickness
ϵ = $1 - \kappa$
ζ = dimensionless axial coordinate
η = non-Newtonian viscosity
η_0 = zero shear viscosity
η_∞ = infinite shear viscosity
θ = temperature; angular coordinate
$\langle\theta\rangle$ = average temperature
κ = ratio of radii of inner cylinder to that of outer cylinder
λ^2 = eigenvalues of Equation (43)
ξ = dimensionless radial coordinate; dimensionless rectangular coordinate
ρ = density
ρ^* = dimensionless density
τ = shear stress tensor
$\tau_{1/2}$ = parameter in Equation (2)
τ_B = shear stress at slot wall
τ_R = shear stress at tube wall
χ = thermal diffusivity ($k/\rho \hat{C}_p$)
Ω = angular velocity
Ω^* = dimensionless angular velocity
Ω_i = angular velocity of inner cylinder
Ω_o = angular velocity of outer cylinder

LITERATURE CITED

1. Ashare, E., and R. B. Bird, *A.I.Ch.E. J.*, submitted for publication.
2. Beek, W. J., and R. Eggink, *Ingenieur*, **74**, 81-89 (1962).
3. Biery, J. C., *A.I.Ch.E. Journal*, **10**, 551 (1964).
4. Bird, R. B., manuscript prepared for the First Joint Meeting of A.I.Ch.E. and Inst. of Chem. Engr., London (1965).
5. ———, *Can. J. Chem. Engr.*, to be published.
6. ———, *Chem. Ing. Technik*, **31**, 569 (1959).
7. ———, C. F. Curtiss, and W. E. Stewart, *Chem. Eng. Sci.*, **11**, 114 (1959).
8. ———, W. E. Stewart, and E. N. Lightfoot, "Transport Phenomena," Wiley, New York (1960); fourth corrected printing, p. 62 (1964).
9. Frederickson, A. G., Ph.D. thesis, Univ. of Wisconsin, Madison, Wisconsin (1959).
10. ———, "Principles and Applications of Rheology," p. 88, Prentice-Hall, Englewood Cliffs, New Jersey (1964).
11. ———, and R. B. Bird, *Ind. Eng. Chem.*, **50**, 347-352 (1958); errata, *Ind. Eng. Chem. Fundamentals*, **3**, 383 (1964).
12. Gee, R. E., and J. B. Lyon, *Ind. Eng. Chem.*, **49**, 956 (1957).
13. Hildebrand, F. B., "Advanced Calculus for Applications," p. 200, Prentice-Hall, Englewood Cliffs, New Jersey (1963).
14. Hohenemser, K., and W. Prager, *Z. Angew. Math. Mech.*, **12**, 216-226 (1932).
15. Lyche, B. C., and R. B. Bird, *Chem. Eng. Sci.*, **6**, 35 (1956).
16. Lyon, R. N., *Chem. Eng. Progr.*, **47**, 75 (1951).
17. McEachern, D. W., Ph.D. thesis, Univ. of Wisconsin, Madison, Wisconsin (1963).
18. McEachern, D. W., manuscript prepared for A.I.Ch.E. Meeting in Houston, Texas (February 1965).

19. Meter, D. M., Ph.D. thesis, Univ. of Wisconsin, Madison, Wisconsin (1963).
20. ———, *A.I.Ch.E. Journal*, **10**, 881-884 (1964).
21. ———, and R. B. Bird, *ibid.*, 878-881.
22. Reiner, M., "Deformation, Strain, and Flow," Interscience, New York (1960).
23. Sadowski, T. J., Ph.D. thesis, Univ. of Wisconsin, Madison, Wisconsin (1963).
24. Slattery, J. C., Ph.D. thesis, Univ. of Wisconsin, Madison, Wisconsin (1959).
25. ———, and R. B. Bird, *Chem. Eng. Sci.*, **16**, 231-241 (1961).
26. Sneddon, I. N., "Elements of Partial Differential Equations," p. 49, McGraw-Hill, New York (1957).
27. Spriggs, T. W., Ph.D. thesis, Univ. of Wisconsin, Madison, Wisconsin (1965).
28. ———, *Chem. Eng. Sci.*, **20** (1965).
29. ———, and R. B. Bird, *Ind. Eng. Chem. Fundamentals*, **4**, 182-186, (1965).
30. Sutterby, J. L., Ph.D. thesis, Univ. of Wisconsin, Madison, Wisconsin (1964).
31. Turian, R. M., Ph.D. thesis, Univ. of Wisconsin, Madison, Wisconsin (1964).
32. Turian, R. M., *Chem. Eng. Sci.*, **20** (1965).
33. Williams, M. C., and R. B. Bird, *Phys. of Fluids*, **5**, 1126 (1962); **6**, 314 (1963).
34. ———, *Ind. Eng. Chem. Fundamentals*, **3**, 42-49 (1964).

Manuscript received August 25, 1964; revision received December 21, 1964; paper accepted December 23, 1964.

Flash X-Ray Analysis of Fluidized Beds

JACOB B. ROMERO and DON W. SMITH

The Boeing Company, Seattle, Washington

Flash X-ray radiography was used to study the internal structure of fluidized beds. Basic data were obtained on the density distribution and on void shapes, sizes, and velocities within an air-sand bed. The data obtained, in general, support the view of fluidized beds as consisting of liquidlike emulsions through which voids rise. Density measurements and void characteristics were in agreement with the two-phase flow theory and with more recent theories of fluid bed flow. Void velocities and shapes agreed with recent predictions that the dense phase behaves as a liquidlike emulsion of zero viscosity and surface tension.

A fruitful model of a gas fluidized bed depicts it as consisting of a stable, liquidlike dense phase through which voids rise. The void maintains its integrity through gas circulation that enters through its base and exits through its roof and sides. Essentially, all fluid not required to fluidize the bed bypasses the bed in the form of voids. This concept has contributed greatly to a basic understanding of the fluidized bed. It is now possible to predict many properties of the fluid bed—mode of fluidization (*1*), bed stability (*2*), void movement (*3, 4*), and solid mixing (*5*)—with a fair degree of success.

The model of the fluidized bed described above combines the simplicity of the two-phase flow theory (*6*) with theories to account for void stability and flow. The main purpose of the present study was to obtain experimental data in support of these theories through a study of dense- and dilute-phase characteristics. For example, a knowledge of density distribution should provide evidence for the validity of the two-phase flow theory. Also, measurements of bubble shapes, sizes, and velocities should help support theories on flow of voids through fluidized solids.

Previous experiments on fluidized beds have, in general, supported this model, but have also counted heavily on observations near the wall surfaces of fluidized beds and on probe measurements inserted into the bed. The latter measurements have used capacitance probes (*7*), light probes (*8*), and localized X-ray beams (*9*). Dye has been used to produce streak lines around voids in two-dimensional beds and thereby illustrate the flow pattern (*10*). Bubble velocities have been measured by introducing gas pulses, which are not indigenous to the bed, into a bed held just above minimum fluidization (*11, 12*).

In the present study, flash X-ray radiography was used to study the internal structure of fluidized beds (*13*). In this manner, the motion within the bed was stopped, and it was possible to observe conditions existing within a large section of the bed without disturbing the bed in any manner. Flash X-ray photographs yielded data on density distribution, bubble sizes, and bubble shapes. Two flash units fired in sequence permitted measurement of the velocity of bubbles as they rise through the bed. The flash X-ray machine has an extremely fast exposure time; this feature can be used to advantage in experiments where fast motion has to be resolved. Previous applications of flash X-ray include the resolution of motion of bullets, expansion of exploding wires, and displacement of internal organs during acceleration (*14*).

The work was essentially statistical. To obtain data on bubble sizes, for instance, many measurements were undertaken to obtain a statistical average. Because of these and other considerations, this work was limited to an air-sand system and to one column size. The results, which support many previous theories, should prove valuable for a basic understanding of fluidized beds and should provide useful data for fluid bed design.

EXPERIMENTAL

Apparatus

Two existing flash X-ray facilities were used to obtain photographs of the bed internals. These units, which are designed for 300- and 600-kv. operation, could easily penetrate a few inches of solid fluidized material. Except for experiments involving void velocity measurements, only the 300-kv. unit was used.